Optics Letters

Efficient continuous-wave Nd:YVO_4/KGW intracavity Raman laser

JINGNI GENG,[1,2] QUAN SHENG,[1,2,3] SHIJIE FU,[1,2] WEI SHI,[1,2,4] AND JIANQUAN YAO[1,2]

[1]Institute of Laser and Optoelectronics, School of Precision Instrument and Optoelectronics Engineering, Tianjin University, Tianjin 300072, China
[2]Key Laboratory of Optoelectronic Information Technology (Ministry of Education), Tianjin University, Tianjin 300072, China
[3]shengquan@tju.edu.cn
[4]shiwei@tju.edu.cn

Received 14 August 2023; revised 25 October 2023; accepted 31 October 2023; posted 1 November 2023; published 4 December 2023

We demonstrate an efficient Nd:YVO_4/KGW intracavity Raman laser in continuous-wave (CW) scheme. With a V-shaped fundamental laser cavity and a short Stokes cavity in it, the oscillating beam sizes are designed to alleviate the thermal effect and to enhance the Raman gain for efficient CW operation. The output power of CW Stokes wave at 1177 nm reached 9.33 W under an incident laser diode pump power of 36.65 W, with corresponding optical efficiency being 25.5%. To the best of our knowledge, these are the highest Stokes output power and conversion efficiency of CW intracavity Raman lasers.

https://doi.org/10.1364/OL.503201

Crystalline Raman lasers based on stimulated Raman scattering (SRS) in nonlinear crystals have long been established as an effective technique for wavelength-versatile output from ultraviolet to mid-infrared [1–4]. Due to the relatively low $\chi^{(3)}$ nonlinear gain, Raman lasers usually suffer a high SRS threshold when operating in the continuous-wave (CW) regime. Even when expensive novel high-gain Raman crystals like diamond are used, the SRS would occur only when the pump power reached 20 W level [5,6], which makes the laser inefficient for low-to-moderate power applications. An alternative approach for efficient CW Raman output is the intracavity pumping scheme, in which the Raman crystal is located inside the cavity of the fundamental laser, so that the high circulating power at fundamental wavelength in the cavity would produce sufficient gain for CW SRS with watt-level primary laser diode (LD) pump power [7–9]. Efficient intracavity Raman lasers (including self-Raman lasers) with multi-watt CW Stokes output and/or its second-harmonic have been demonstrated by many groups [7,10,11].

While the circulating fundamental power makes it easy to reach the SRS threshold, the power/efficiency of intracavity Raman lasers are still very sensitive to cavity losses, since the low SRS gain only allows for the output coupling of a few percent or lower [12]. Another issue hindering the power scaling of intracavity Raman lasers is the thermal effect. Both processes of fundamental wave lasing and SRS bring heavy thermal load; therefore, the onset of cavity instability induced by strong thermal lenses often limits the maximum pump power allowed. Therefore, to minimize the loss and enhance the resistance to thermal lens effect, the majority of the CW intracavity Raman lasers reported are with short, linear cavity [7,8,11–14]. In 2010, researchers at Macquarie University reported a 4.3 W CW yellow output at 586 nm by intracavity frequency-doubling the 1173 nm Stokes wave of an end-pumped Nd:$GdVO_4$ self-Raman laser with a cavity length of only 35 mm [14]. With a double-end pumping scheme to alleviate the thermal effect, the same group demonstrated a 4.05 W CW Stokes output later [15]. The instantaneous output power when operated in quasi-continuous-wave (QCW) pumping scheme reached 5.63 W. The highest end-pumped CW intracavity Raman Stokes output was demonstrated by Fan *et al.* in 2016, via a self-Raman scheme [7]. The laser with a 20 mm long YVO_4–Nd:YVO_4–YVO_4 crystal and a short cavity length of only 23 mm generated a 5.3 W 1176 nm two-way output under an incident LD pump power of 26 W. For the side-pumped scheme in which a higher pump power can be used, Savitski *et al.* have demonstrated a higher CW Stokes output of 6.1 W from an Nd:YLF/KGW intracavity Raman laser under 150 W LD pump [16]. More recently, Chen *et al.* demonstrated a 6.8 W 579.5 nm output by intracavity frequency-doubling the 1159 nm first Stokes of a Nd:YVO_4/KGW Raman laser [11]. Later, with optimized crystal coatings to minimize the loss and cavity length of a Nd:$GdVO_4$/KGW Raman laser, the same group realized a 3.1 W CW output and a 10.5 W QCW instantaneous output at 578 nm [17].

Compared with self-Raman lasers, the intracavity Raman lasers with separate laser and Raman crystals benefit from more flexible output wavelength, as well as the potential for greater power scaling due to the distributed thermal load between the two crystals [13]. The scheme with separate laser and Raman crystals also allows for separate fundamental and Stokes cavities, which is more convenient for power and efficiency scaling. For example, one can use large mode sizes in the laser gain medium to control the thermal issues, while small mode sizes can be used at the Raman crystal for higher nonlinear gain [13]. The separate cavity is also preferred when additional wavelength/frequency selection elements are needed for wavelength-tunable and narrow-linewidth output [1,10,18,19]. The narrowed fundamental and Stokes spectral linewidths could also enhance the power and efficiency of the CW intracavity Raman lasers significantly [10,18,19]. In this work, we report

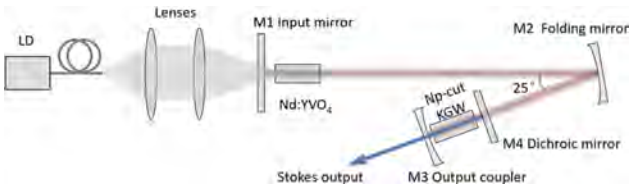

Fig. 1. Schematic of the Nd:YVO_4/KGW intracavity Raman laser.

the first demonstration of CW intracavity Raman laser with 10 W-level Stokes output. With a V-shaped 1064 nm Nd:YVO_4 fundamental laser cavity and a short KGW Raman cavity in it, the oscillating beam sizes were designed to alleviate the thermal effect and to enhance the Raman gain for efficient CW operation. The CW 1177 nm Stokes output power reached 9.33 W under an incident LD pump power of 36.65 W, with corresponding optical efficiency being 25.5%, which are the highest Stokes output power and optical efficiency of the CW intracavity Raman laser reported. The power and spectral behavior with fundamental laser polarization along different axes of the N_p-cut KGW crystal were also investigated.

The experimental arrangement of the CW intracavity Raman laser is depicted in Fig. 1. The pump source is a fiber-coupled LD at 878.6 nm. The pump light was delivered from a fiber with a core diameter of 200 μm and a numerical aperture of 0.22 and was refocused by a pair of lenses onto the front facet of the laser crystal with a beam radius of 280 μm. The laser crystal was an *a*-cut Nd:YVO_4 crystal (CASTECH Inc.) with a low doping concentration of 0.2 at. % and dimensions of 3 mm × 3 mm × 15 mm; both facets of which were coated for anti-reflective (AR) at 878.6 nm and 1064 nm. The crystal was measured to absorb ~79% of the incident non-polarized pump under non-lasing conditions. The 1064 nm fundamental laser cavity was defined by a flat input mirror M1 and two concave mirrors M2 and M3, each having radii of curvature of 100 mm. M1 was coated for AR at 878.6 nm ($R < 0.5\%$) and highly reflective (HR) at 1064 nm ($R > 99.9\%$). M2 was coated for HR at 1064 nm ($R = 99.97\%$) to fold the cavity with a full folding angle of ~25°, while the Stokes output coupler M3 was coated for HR at 1064 nm ($R > 99.99\%$) and partially transmissive ($T = 0.4\%$) at 1177 nm. The Raman gain medium was a 20 mm-long KGW crystal (CASTECH Inc.) cut along its N_p axis. The crystal was coated for AR at the fundamental ($R < 0.2\%$) and the Stokes ($R < 0.1\%$) wavelengths on both facets. A flat dichroic mirror M4 coated for HR at 1177 nm ($R > 99.96\%$) and AR at 1064 nm ($R < 0.2\%$) was inserted into the fundamental cavity to make the Stokes cavity with M3. The distances M1–M2 and M2–M3 were 168 mm and 65 mm, respectively. The distances between the Nd:YVO_4 crystal and the input mirror M1 and between the KGW crystal and the output coupler M3 were both ~3 mm. The length of the Stokes cavity M3–M4 was ~26 mm. Both of the two crystals were wrapped in indium foil and mounted in aluminum holders water-cooled at 20°C.

In this cavity arrangement, the TEM_{00} mode sizes of 1.06 μm fundamental laser were calculated (based on the *ABCD* matrix using reZonator software) to be 280 × 260 μm (radii) in the laser crystal and 60–90 μm in the Raman crystal for the cold cavity, while the TEM_{00} mode radius of the 1.18 μm Stokes wave was 115–120 μm in the KGW crystal. For intracavity Raman lasers, the fundamental lasers usually operate in multi-transverse mode because the coupling from fundamental field to Stokes wave

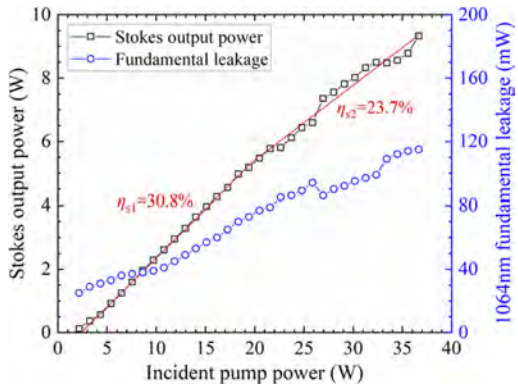

Fig. 2. CW 1177 nm Stokes output power and a 1064 nm fundamental leakage versus an incident LD pump power with fundamental polarization $E//N_m$.

acts as a strong nonlinear loss on its fundamental transverse mode. Therefore, the TEM_{00} mode radius of the Stokes wave was designed to be a bit larger than that of the fundamental laser, to make full use of the multi-transverse-mode fundamental laser.

We first oriented the crystals to have the 1064 nm fundamental laser polarized parallel to the N_m axis of the KGW crystal (perpendicular to the table), to make use of the 901 cm^{-1} Raman line (Raman gain coefficient g_R of ~6 cm/GW, over two times stronger than the 768 cm^{-1} line with this polarization [20]). Figure 2 plots the Stokes output power as a function of incident LD pump power, measured using a laser powermeter Ophir NOVA II with sensor 30A-BB-18. The pump threshold for SRS was below 2 W incident LD power, and the Stokes output power reached 9.33 W under the maximum incident pump power used of 36.65 W, with an optical efficiency being 25.5%. To the best of our knowledge, these are the highest Stokes output power and conversion efficiency of CW intracavity Raman lasers, including the self-Raman scheme. Considering the fractional pump absorption of 79%, the conversion efficiency with respect to the absorbed pump power was 32.2%. The laser output power did not exhibit any roll over, and only the first Stokes output centered at 1177.3 nm was observed during the whole process except for very weak (peak intensity over 20 times lower than that of the 1177.3 nm Stokes) cascaded Stokes at 1193.2 nm and 1206.5 nm (which corresponded to 113 cm^{-1} and 205 cm^{-1} Raman lines, respectively, from 1177.3 nm first Stokes [21]) when the output power was beyond 9 W. According to the *ABCD* matrix calculation, the shortest thermal lens focal length f_t in the Nd:YVO_4 crystal allowed before the onset of fundamental laser cavity instability was ~140 mm, which revealed that the f_t was still beyond this value. The thermal issues were well alleviated by using the Nd:YVO_4 crystal with the low doping concentration of 0.2 at. % here. We did not further increase the pump power to avoid the risk of components damage considering the rather low Stokes output coupling of 0.4% and the resultant high circulating Stokes power of over 2 kW (one way) in the cavity. Given the low SRS threshold, higher Stokes output coupling can be used for higher slope efficiency and resultant output power, as well as to decrease the intracavity Stokes power to avoid the cascaded SRS processes. Figure 2 also shows the leakage of the 1064 nm fundamental laser (blue circles) recorded behind mirror M2 (using a laser power meter Ophir VEGA with sensor 12A), which increased from 25 mW at the SRS threshold to 115 mW at the maximum pump power. Using the measured

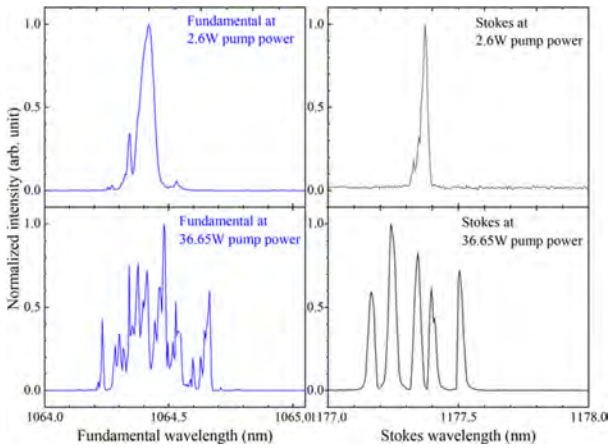

Fig. 3. Typical fundamental and Stokes spectra at different powers ($E//N_m$).

transmittance of $T_{M2} = 0.03\%$ at 1064 nm, we can estimate the intracavity fundamental power, which was ~80 W (one way) at the SRS threshold and increased to near 400 W at the maximum pump power.

The fundamental and Stokes spectra under different pump power were recorded using an optical spectrum analyzer (OSA) Yokogawa 6370d with a resolution of 0.02 nm. As shown in Fig. 3, the spectral linewidth of the 1064.4 nm fundamental laser was 0.06 nm at the pump of 2.6 W (just above SRS threshold) and was broadened to over 0.3 nm (2.7 cm^{-1}) when operated with the maximum Stokes output power of 9.33 W. Correspondingly, the Stokes linewidth was broadened from below 0.03 nm to ~0.35 nm (2.5 cm^{-1}). Since the spontaneous Raman linewidth $\Delta\nu_R$ of the 901 cm^{-1} Raman line of KGW (5.4 cm^{-1}) is comparable to the spontaneous emission linewidth of the *a*-cut Nd:YVO_4 crystal (9.7 cm^{-1}), such degree of the spectral broadening of the 1064 nm fundamental laser was mainly due to the spatial hole burning, rather than the SRS-induced spectrally varying loss [19]. The spectral broadening would be much more serious if crystals with narrower $\Delta\nu_R$ were used as Raman gain medium. However, the broadening of fundamental and Stokes spectra here is already significant enough to decrease the effective Raman gain coefficient g_{R_eff} [12,19]. Using Eq. (2) in [18] and the spectra in Fig. 3, the g_{R_eff} at the maximum power was calculated to be only ~45% of that at the SRS threshold. This can well explain the change of laser slope efficiency shown in Fig. 2. The slope efficiency with the pump power below 20 W was up to 30.8% but decreased to 23.7% under pump power beyond 20 W. Another observation related to this is the increase of the 1064 nm leakage plotted in Fig. 2. With decreasing g_{R_eff}, the CW Raman laser requires a higher fundamental intensity to keep the round-trip Raman gain at the threshold level; therefore the leakage increased with higher pump power. Therefore, enhanced Stokes output power and conversion efficiency can be expected if frequency-selection element like etalon is used to control the laser linewidth [10,18,19].

Figure 4 shows some typical beam profiles of the fundamental leakage and the Stokes output recorded using a CCD camera Ophir SP907. The fundamental laser was operating in fundamental transverse mode with incident pump power below SRS threshold [Fig. 4(a)] and started to degrade after the SRS occurred, as shown in Figs. 4(b)–4(e). Meanwhile, the Stokes output had a good beam quality with pump power below 15 W

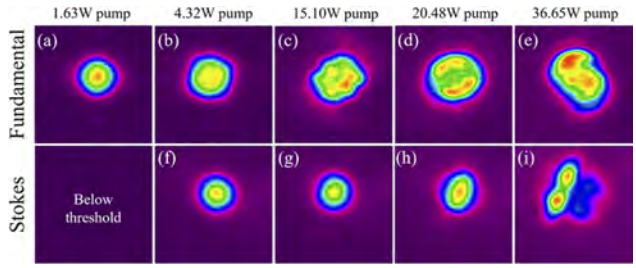

Fig. 4. Beam profile evolution with a pump power ($E//N_m$).

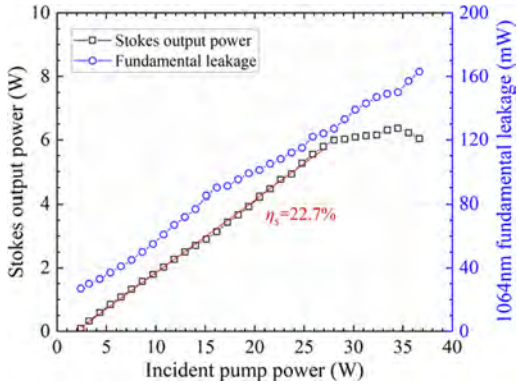

Fig. 5. Stokes output power and a 1064 nm fundamental leakage versus an incident LD pump power with fundamental polarization $E//N_g$.

(4 W output) because of the beam cleanup effect of the SRS process and well-designed mode matching, despite the distorted fundamental beam profiles, as shown in Figs. 4(f) and 4(g). However, the Stokes beam profile became elliptical at a higher power [Fig. 4(h)] and finally operated in a high-order Hermit–Gaussian mode [Fig. 4(i)], because of the astigmatic thermal lens in the KGW [22]. It can be seen that the axes of the elliptical and Hermit–Gaussian modes did not overlap with the N_m/N_g axes of the crystal (which are perpendicular and parallel to the table, respectively), because the thermal expansion axes are offset from the optical axes [22].

For comparison, we also oriented the Raman crystal to have fundamental polarization $E//N_g$. As shown in Fig. 5, in this case, the Stokes output power was much lower than that with $E//N_m$. The laser had a slope efficiency of 22.8% with a pump power below 27 W, after which the Stokes power increase became quite slow. The maximum Stokes output power was only 6.36 W, obtained under the incident pump power of 34.5 W. Then the roll over occurred when further increasing the pump power, though the fundamental leakage kept growing. Using the OSA, we found that the Raman output contained both 1159.2 nm and 1177.3 nm components, which corresponded to the 768 cm^{-1} and 901 cm^{-1} Raman lines, respectively. The two Stokes lines started oscillating simultaneously at the incident pump power of ~2.4 W and had similar intensities on the OSA when the output power was below 1 W. As the pump increased, the 1159.2 nm Stokes dominated the Stokes output gradually, which was 3–5 times higher than the 1177.3 nm line at the maximum power. The two Stokes lines divided the Raman gain hence resulting in a decreased conversion efficiency. The 1064 nm fundamental leakage at the SRS threshold was higher than that of $E//N_m$ case and grew faster

compared with the curve in Fig. 2 and revealed that the conversion from the fundamental field to the Stokes wave was less efficient because of the lower Raman gain. Since the 768 cm^{-1} Raman line has a linewidth (6.4 cm^{-1}) wider than that of the 901 cm^{-1} Raman line, the spectral linewidth of the 1159.2 nm Stokes was even a little broader (~0.45 nm at the maximum power) than that of the 1177.3 nm Stokes output at the maximum output power of 9.33 W obtained with $E//N_m$. Because the KGW crystal also exhibits quite strong 89 cm^{-1} Raman gain when $E//N_g$, weak Stokes lines at 1170.7 nm and 1189.2 nm, which corresponded to the cascaded Raman shift from 1159.2 nm and 1177.3 nm first Stokes lines, were also observed after the output power reached 1.5 W and 2 W, respectively. The intensity of the 1170.7 nm and 1189.2 nm lines were 5–10 times lower than those of the 1159.2 nm and 1177.3 nm output, respectively, seen from the OSA. Therefore, the $E//N_g$ arrangement is not suitable for efficient single-wavelength Raman output compared with the $E//N_m$ arrangement, unless the coatings are specially optimized to suppress the Stokes lines unwanted.

In summary, we demonstrated an efficient Nd:YVO_4/KGW intracavity Raman laser in CW scheme. A coupled folded cavity was designed to control the beam sizes in the laser crystal and Raman crystal, to alleviate the thermal issues and enhance the Raman gain. With the fundamental laser polarized along N_m axis of the N_p-cut KGW crystal, 9.33 W first Stokes output at 1177.3 nm was obtained under an incident LD pump power of 36.65 W, with an optical efficiency of 25.5%. Our results show that the compact intracavity Raman laser is capable of generating a 10 W-level CW output efficiently via an appropriate cavity design. The influences of fundamental polarization on the power and spectral behavior of the Raman laser were also investigated.

Funding. National Natural Science Foundation of China (61975146, 62075159, 62105240, 62275190).

Acknowledgment. The authors acknowledge Prof. Helen M. Pask at Macquarie University for the helpful discussions and language editing.

Disclosures. The authors declare no conflicts of interest.

Data availability. Data underlying the results presented in this paper are not publicly available at this time but may be obtained from the authors upon reasonable request.

REFERENCES

1. R. Casula, J. Penttinen, M. Guina, A. J. Kemp, and J. E. Hastie, Optica **5**, 1406 (2018).
2. H. M. Pask, P. Dekker, R. P. Mildren, D. J. Spence, and J. A. Piper, Prog. Quantum. Electron. **32**, 121 (2008).
3. H. Zhao, C. Lin, C. Jiang, S. Dai, H. Zhou, S. Zhu, H. Yin, Z. Li, and Z. Chen, Opt. Express **31**, 265 (2023).
4. Y. Duan, Y. Sun, H. Zhu, T. Mao, L. Zhang, and X. Chen, Opt. Lett. **45**, 2564 (2020).
5. O. Lux, S. Sarang, O. Kitzler, D. J. Spence, and R. P. Mildren, Optica **3**, 876 (2016).
6. Y. Sun, M. Li, O. Kitzler, R. P. Mildren, Z. Bai, H. Zhang, J. Lu, Y. Feng, and X. Yang, Laser Phys. Lett. **19**, 125001 (2022).
7. L. Fan, W. Zhao, X. Qiao, C. Xia, L. Wang, H. Fan, and M. Shen, Chin. Phys. B **25**, 114207 (2016).
8. X. Li, A. J. Lee, H. M. Pask, J. A. Piper, and Y. Huo, Opt. Lett. **36**, 1428 (2011).
9. C. Y. Lee, C. Chang, P. H. Tuan, C. Y. Cho, K. F. Huang, and Y. F. Chen, Opt. Lett. **40**, 1996 (2015).
10. Q. Sheng, R. Li, A. J. Lee, D. J. Spence, and H. M. Pask, Opt. Express **27**, 8540 (2019).
11. Y. F. Chen, C. M. Chen, C. C. Lee, H. Y. Huang, D. Li, J. Q. Hsiao, C. H. Tsou, and H. C. Liang, Opt. Lett. **45**, 5612 (2020).
12. D. J. Spence, IEEE J. Select. Topics Quantum Electron. **21**, 134 (2015).
13. A. J. Lee, H. M. Pask, J. A. Piper, H. Zhang, and J. Wang, Opt. Express **18**, 5984 (2010).
14. A. J. Lee, D. J. Spence, J. A. Piper, and H. M. Pask, Opt. Express **18**, 20013 (2010).
15. J. Lin and H. M. Pask, Appl. Phys. B **108**, 17 (2012).
16. V. G. Savitski, I. Friel, J. E. Hastie, M. D. Dawson, D. Burns, and A. J. Kemp, IEEE J. Quantum Electron. **48**, 328 (2012).
17. Y. F. Chen, D. Li, Y. M. Lee, C. C. Lee, H. Y. Huang, C. H. Tsou, and H. C. Liang, Opt. Lett. **46**, 797 (2021).
18. G. M. Bonner, J. Lin, A. J. Kemp, J. Wang, H. Zhang, D. J. Spence, and H. M. Pask, Opt. Express **22**, 7492 (2014).
19. Q. Sheng, A. J. Lee, D. J. Spence, and H. M. Pask, Opt. Express **26**, 32145 (2018).
20. I. V. Mochalov, Opt. Eng. **36**, 1660 (1997).
21. L. Macalik, J. Hanuza, and A. A. Kaminskii, J. Raman Spectrosc. **33**, 92 (2002).
22. A. M. Mckay, O. Kitzler, and R. P. Mildren, Opt. Express **22**, 707 (2014).